Opto-Electronic Advances

Original Article

2022, Vol. 5, No. 9

DOI: 10.29026/oea.2022.210069

Photonic synapses with ultralow energy consumption for artificial visual perception and brain storage

Caihong Li[1], Wen Du[1], Yixuan Huang[1], Jihua Zou[1], Lingzhi Luo[1], Song Sun[2,3], Alexander O. Govorov[4], Jiang Wu[1,5]*, Hongxing Xu[1,6] and Zhiming Wang[1]

The human visual system, dependent on retinal cells, can be regarded as a complex combination of optical system and nervous system. Artificial retinal system could mimic the sensing and processing function of human eyes. Optically stimulated synaptic devices could serve as the building blocks for artificial retinas and subsequent information transmission system to brain. Herein, photonic synaptic transistors based on polycrystalline MoS_2, which could simulate human visual perception and brain storage, are presented. Moreover, the photodetection range from visible light to near-infrared light of MoS_2 multilayer could extend human eyes' vision limitation to near-infrared light. Additionally, the photonic synaptic transistor shows an ultrafast speed within 5 μs and ultralow power consumption under optical stimuli about 40 aJ, several orders of magnitude lower than biological synapses (50 ms and 10 fJ). Furthermore, the backgate control could act as emotional modulation of the artificial brain to enhance or suppress memory function, i.e. the intensity of photoresponse. The proposed carrier trapping/detrapping as the main working mechanism is presented for the device. In addition, synaptic functionalities including short synaptic plasticity, long synaptic plasticity and paired-pulse facilitation could be successfully simulated based on the prepared device. Furthermore, the large difference between short synaptic plasticity and long synaptic plasticity reveals the better image pre-processing function of the prepared photonic synapses. The classical Pavlovian conditioning associated with the associative learning is successfully implemented as well. Therefore, the efficient and rich functionalities demonstrate the potential of the MoS_2 synaptic device that integrates sensing-memory-preprocessing capabilities for realizing artificial neural networks with different emotions that mimic human retina and brain.

Keywords: MoS_2 synaptic transistors; visual perception; ultralow power consumption; memory

Li CH, Du W, Huang YX, Zou JH, Luo LZ et al. Photonic synapses with ultralow energy consumption for artificial visual perception and brain storage. *Opto-Electron Adv* **5**, 210069 (2022).

[1]Institute of Fundamental and Frontier Sciences, University of Electronic Science and Technology of China, Chengdu 610054, China; [2]Microsystem and Terahertz Research Center, China Academy of Engineering Physics, Chengdu 610200, China; [3]Institute of Electronic Engineering, China Academy of Engineering Physics, Mianyang 621999, China; [4]Department of Physics and Astronomy, Ohio University, Athens, Ohio 45701, United States; [5]State Key Laboratory of Electronic Thin Films and Integrated Devices, University of Electronic Science and Technology of China, Chengdu 610065, China; [6]School of Physics and Technology, Wuhan University, Wuhan 430072, China.

*Correspondence: J Wu, E-mail: jiangwu@uestc.edu.cn

Received: 28 May 2021; Accepted: 6 October 2021; Published online: 25 June 2022

Introduction

Researches on artificial neural networks (ANN) which could offer both storage and computing have been carried out extensively in order to obtain a deeper understanding of human vision and brain[1,2]. For example, synaptic transistors, memristors[3], phase change memories, etc. have been widely applied to simulate biological neurons[4–6]. Furthermore, the spiking neural networks (SNN), as the third generation of ANN, are the biologically-realistic models of living nervous systems taking discrete events instead of continuous values as stimuli[7]. From a single device to an array of devices, increased number of more complex functions could be realized, such as the field of artificial intelligence (AI) related to vision[8–11]. In addition, associative learning based on the interaction between thoughts and experience is one of the most important capabilities of human brain cells[12]. The classical Pavlovian conditioning links two stimuli together to produce a new learned response in a person or animal[13]. Recently, different materials and various structures are used to stimulate the effective performance of biological synapses[1,14,15]. The main significant figure of merit are sensitivity and power consumption for evaluating neural devices[16]. The ideal synaptic transistors have strong synaptic plasticity and lower power consumption than biosynapses which consumes about 10 fJ per spike[1,17,18]. Synaptic plasticity is divided into long-term synaptic plasticity (LTP) closely related to learning and memory and short-term synaptic plasticity (STP) processing the temporal information on the relevant time scales such as milliseconds or seconds[12,17]. According to Hebbian theory, also called spike timing-dependent plasticity (STDP), persistent or repeated stimuli give rise to a higher synaptic weight which represents the strength of connection between two nodes[19–21]. In addition, spike-duration dependent plasticity, spike-number dependent plasticity, spike-frequency dependent plasticity, learning-experience behavior and forgetting behavior are also important parameters to measure the properties of synaptic devices[17,22].

Photonic synapses, coupling optical sensing and synaptic plasticity, are expected to reduce power consumption and achieve ultrafast signal transmission[23,24]. The light-sensitive photosensors are similar to the photoreceptors of biological retina because they both can convert light signals to electrical signals[25]. This kind of devices, which could mimic the biologic eyes and work as a standalone platform, would pave the way for machine vision systems in the future[26]. Moreover, Lee's group have extended the human visual sense beyond visible light to UV light and this work may be further applied to healthcare via combining UV selectivity and dose-calculation[27].

Optical modulation as a novel gate-control mode for achieving multi-terminal neuromodulations could decrease thermal loss and operate simply[17]. The light-stimulated synaptic device offers more possibilities to broaden the functionalities and system complexities of the current neuromorphic systems[24]. Two-dimensional (2D) transition metal dichalcogenides (TMDs) are intriguing and promising optoelectronic devices due to their superb electrical and optical properties[28,29]. Many kinds of 2D TMDs could be synthesized in large-area by chemical vapor deposition (CVD) or other methods, making practical devices possible[30–34]. Molybdenum disulfide (MoS_2) has been investigated as an efficient charge-trapping layer and light absorption layer in photonic synapses recently due to fast charge-trapping rate, good trapped charge-retention, good optical absorption[35,36] and high carrier mobilities[1,17,18,37,38]. Yoo's group[37] has confirmed that the MoS_2 layer could act as a high-efficiency charge-trapping layer via control experiment. Although the two-terminal devices are easier to form a crossbar-array structure, the inhibitory synaptic behaviours cannot be achieved in these devices[39]. Furthermore, three-terminal gate-control synaptic transistors are able to possess another degree-of-freedom to modulate the neuromorphic function apart from optical modulation[8,40]. For instance, Chu's group[40] have shown a gate tunable artificial synapse to mimic the modulation of drug dosage. In addition, MoS_2 with intrinsic flexibility could be applied to curved image sensor array for the machine vision[41].

The proposed mechanism for photonic synapses is charge trapping/detrapping or phase change[5,39]. The former could achieve low-energy consumption instead of the requirement of high power supplies for the latter[39]. In addition, the trap centers capturing and releasing carriers could be material defects, surface dangling bonds, potential wells[35], etc[42]. The persistent photocurrent/photoconductivity caused by these trap centers make the device be able to mimic some specific functions of biological synapses[26]. Given that, the TMDs with outstanding photoelectric conversion properties and various defects as carrier traps show great potential acting as optically

active layers for photonic synapses[39]. Additionally, the von Neumann bottleneck caused by separated memory units and processing makes synaptic devices with low power consumption more desired[43]. However, electrical synapses under low-energy consumption[17] could be achieved via ultrashort electrical pulses while the photonic synapses with ultralow power consumption to attojoule (aJ) level are still few, especially via ultrashort optical pulses[44].

In this work, the large-area growth 2D MoS_2 films and an array of MoS_2 synaptic transistors integrating the sensing-memory-preprocessing capabilities are demonstrated. The photosensing scope of our devices broadens humanoid vision to near-infrared light. Moreover, the photonic synapses under visible light possess hypersensitivity to transient single pulse and ultralow power consumption superior to bio-synapses. Specifically, the synaptic plasticity via photoinduced charge transfer is investigated including STP, LTP, paired-pulse facilitation (PPF) and the forgetting behavior[23]. The classical Pavlovian conditioning can also be verified by our synaptic device. In addition, back-gate bias could enhance or reduce memory function exhibiting similar effects of emotions[25]. Positive emotions offer a positive effect and vice versa. The image pre-processing is achieved by the large contrast between STP and LTP. Given that, we can conclude such synaptic devices are promising building blocks in AI, especially visual perception and brain storage[26,27,45].

Results and discussion

Synapses, i.e. neuronal junction, could transmit electric nerve impulses between neurons and effectors to achieve signal transmission[17]. In order to mimic the properties of synapses, MoS_2 synaptic transistors are prepared via low pressure CVD (LPCVD) for improved thickness uniformity[34]. The details of material growth and device fabrication are presented in the *Experimental section*. The accurate control of material growth condition including pressure, temperature, the amount of precursors, the position of substrates and so on could improve the reproducibility of channel material. The optical image of the polycrystalline MoS_2 film on a Si/SiO_2 substrate is shown in Fig. 1(a). A continuous and relatively uniform large-area film over 2 cm^2 is grown successfully. Figure 1(b) shows the optical microscopy image of a part of the MoS_2 synaptic transistor array. The devices are fabricated by standard lithography with Ti/Au electrodes as the source, drain, and silicon as the backgate. The corresponding Raman spectrum in Fig. 1(c) shows the typical E_{2g} (381.9 cm^{-1}) and A_{1g} (407.3 cm^{-1}) peaks of MoS_2 measured by the 532 nm laser[28,33,46]. The frequency difference between E_{2g} and A_{1g} is about 25.4 cm^{-1} indicating multilayer growth, which was further confirmed by PL spectrum[47] in Fig. 1(d). Figure 1(e) and 1(f) show the corresponding Raman mapping around 381.4 cm^{-1} and PL mapping selected randomly from Fig. 1(a). The material uniformity of as-grown MoS_2 films can be further confirmed by the uniform color contrast of Raman and PL signals in Fig. 1(e) and 1(f)[48]. Figure 1(g) shows a schematic of the visual perception of human eyes and information transmission to the brain based on our MoS_2 synaptic transistors. The retina in human eyes could detect the visible light and then transmit the information to brain via a number of synapses[27]. Under external stimuli such as optical and electrical pulse, the source and drain electrodes are used to liken pre- and post-synaptic terminals, respectively[25]. Additionally, gate modulation can serve as another form of signal input for three-terminal artificial synapses[8,40].

Photonic synapses which integrate sensing and synaptic function could mimic the visual perception of human retina[27]. The bias voltage (V_{ds}) of 1 V was applied for the following measurements without special instructions. The visible light detection is depicted in Fig. 2(a) and three different wavelengths are chosen including 405 nm, 520 nm and 635 nm. Surprisingly, near-infrared (NIR) light such as 808 nm and 850 nm could also be detected without the upconverting nanoparticles mediation which could upconvert NIR to visible light or UV[18] shown in Fig. 2(b). Because multilayer MoS_2 photodetectors could be responsive to NIR light while monolayer MoS_2 ones could only detect visible light[49,50]. This reveals the capability of photoreception of our device could be extended to NIR as human eyes could only detect the visible light. The broadband detection from visible to NIR light[51] at room temperature based on our MoS_2 synaptic transistors provides new opportunities in machine vision. The insert in Fig. 2(b) shows a good ohmic contact due to linear output characteristics between metal electrodes and MoS_2[14,52–56]. Taking 405 nm laser as an example, synaptic function-related measurements are investigated. Figure 2(c) displays the excitatory post-synaptic current (EPSC, i.e. $I_{ds} - I_{dark}$) of the synaptic device under different single pulse width, showing the spike-duration plasticity[17]. According to Fig. 2(c), the MoS_2

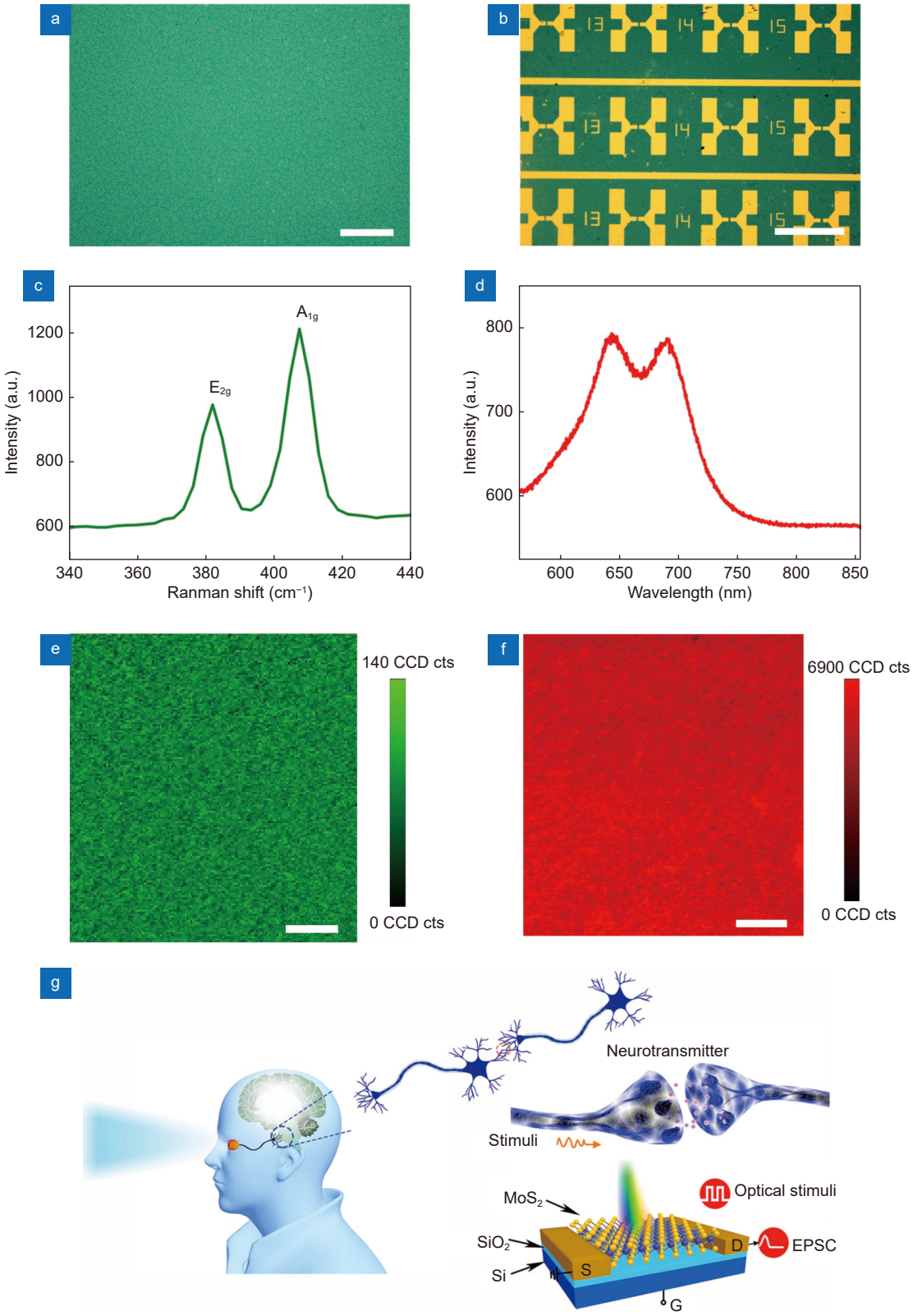

Fig. 1 | Optical characterizations of MoS_2 synaptic transistors and schematic diagram of human eyes. (**a**) The optical image of large-area and uniform polycrystalline MoS_2. Scale bar: 100 μm. (**b**) The optical photograph of a MoS_2 synaptic transistor array on Si/SiO_2 substrate. Scale bar: 500 μm. The corrsponding Raman spectrum (**c**) and PL spectrum (**d**) of MoS_2. The corresponding Raman mapping around 381.4 cm^{-1} (**e**) and PL mapping (**f**) selected randomly from (a). Scale bar: 8 μm. (**g**) Schematic diagram of visual perception and information transmission in human brain and corresponding artifical MoS_2 synaptic device.

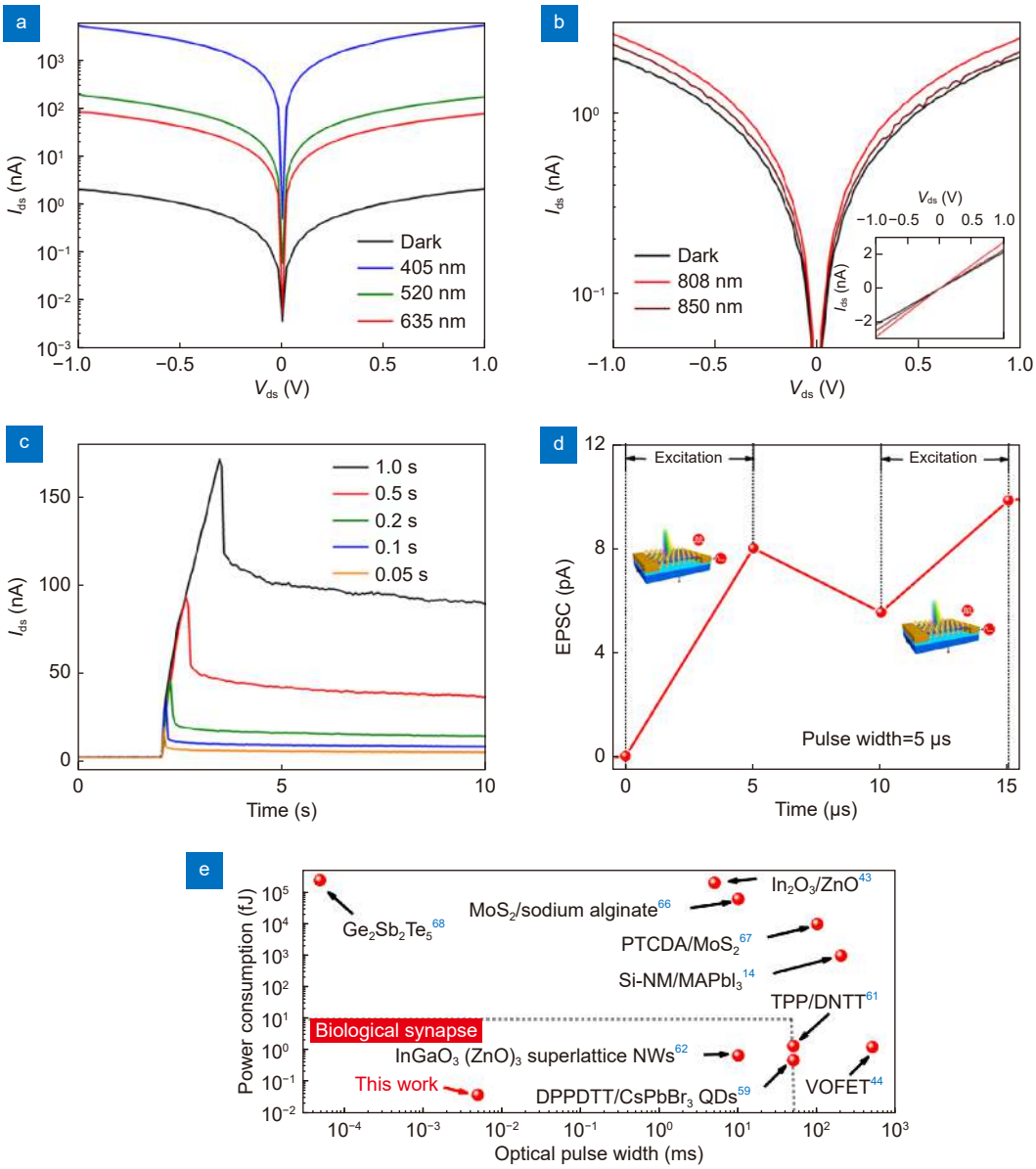

Fig. 2 | Photodetection and spike-duration plasticity of the MoS_2 synaptic transistor. Output characteristic curves of the MoS_2 synaptic transistor in visible light (**a**) and NIR light (**b**). The inset in (b) is the corresponding linear output characteristic curve. (**c**) The transient current responses triggered by several optical stimulus with different duration of a single pulse, respectively. (**d**) The EPSC at the pulse width of 5 μs (405 nm, V_{ds} = 1 V). (**e**) Comparison of single optical pulse width and power consumption among some synaptic devices.

transistor shows typical synaptic properties, i.e. the effects after stimuli do not disappear immediately with the disappearance of the stimuli. The proposed working mechanism based on our photonic synapses is that the charge trapping centers provided by the channel and interfaces reserve the photoinduced carriers even after removing the optical stimuli[57]. That is to say, the persistent photocurrent/photoconductivity phenomenon is attributed to slow recombination of defect or trap centers[35]. The building potential wells between MoS_2 and source-drain electrodes could reserve/release charge carriers with the modulation of light stimuli[35]. The trap sites in the potential wells may originate from the sulfur vacancies in the channel and the dangling Si-O bonds at the interface of MoS_2/SiO_2[35]. The proposed operating process of our photonic synapses might be the state of thermal equilibrium without optical/electrical stimuli at the beginning and generation of photocarrier under optical stimuli followed by carrier trapping, carrier recombination and returning to the original state under dark[43]. In addition, the photocurrent will enhance as the single pulse width prolong obtained from Fig. 2(c) due to the production of more photogenerated carriers. Furthermore, the synaptic transistor distinctly responds to a very

short optical pulse with a width of only 5 μs in Fig. 2(d) which is four orders of magnitude faster than the instantaneous information transmission in the biological synapses (typically 50 ms)[58]. Possible reasons for the ultrashort optical pulse detection capability are ultrafast optical signal propagation speed[2,35,39,59] and ultrasensitive optical detection[60] based on the polycrystalline MoS_2 films. As a result, our synaptic transistors could improve the recognition rate of single optical pulse significantly and achieve an ultralow power consumption of 40 aJ, two orders of magnitude lower than that of biological synapses. The power consumption of one synaptic event could be estimated by the equation of $E = I_{peak} \times V_{read} \times t$ where I_{peak}, V_{read} and t are the maximum EPSC after a pulse, reading voltage and pulse width, respectively[6]. Our power consumption could be reduced by shortening the pulse width with constant reading voltage of 1 V, while many researches achieve low power consumption via decreasing the reading voltage[44,59,61,62] such as 10 μV. So far, the minimum power consumption of a single optical pulse is about femtojoule (fJ) level, well above that of ours (Fig. 2(e))[5,14,17,42–44,59,61–68]. The ultralow power consumption and ultrafast speed suggest the prepared device a promising candidate for an energy-efficient neuromorphic computing system[17].

STP, also called short-term memory (STM), is a critical source information for associative learning and sound localization like classical Pavlovian conditioning[12]. Figure 3(a) shows a clear and typical synaptic response at a single pulse width of 50 ms like the information transmission speed in biological synapses[69] and V_{ds} of 1 V. This optical pulse (405 nm) results in an acute current rise due to a sudden increase of photoinduced carriers[70]. After the optical pulse is off, the EPSC exhibits a slow delay and relatively long relaxation time because the trapped holes by the surface states caused a low recombination rate of carriers[12,70]. Figure 3(b) and inset unfold the EPSC would enhance as the power density (P) of the single optical pulse (width: 100 ms). At the higher P, the faster decay time can be observed in Fig. 3(b) because the decay dynamics are dominated by shallow carrier traps

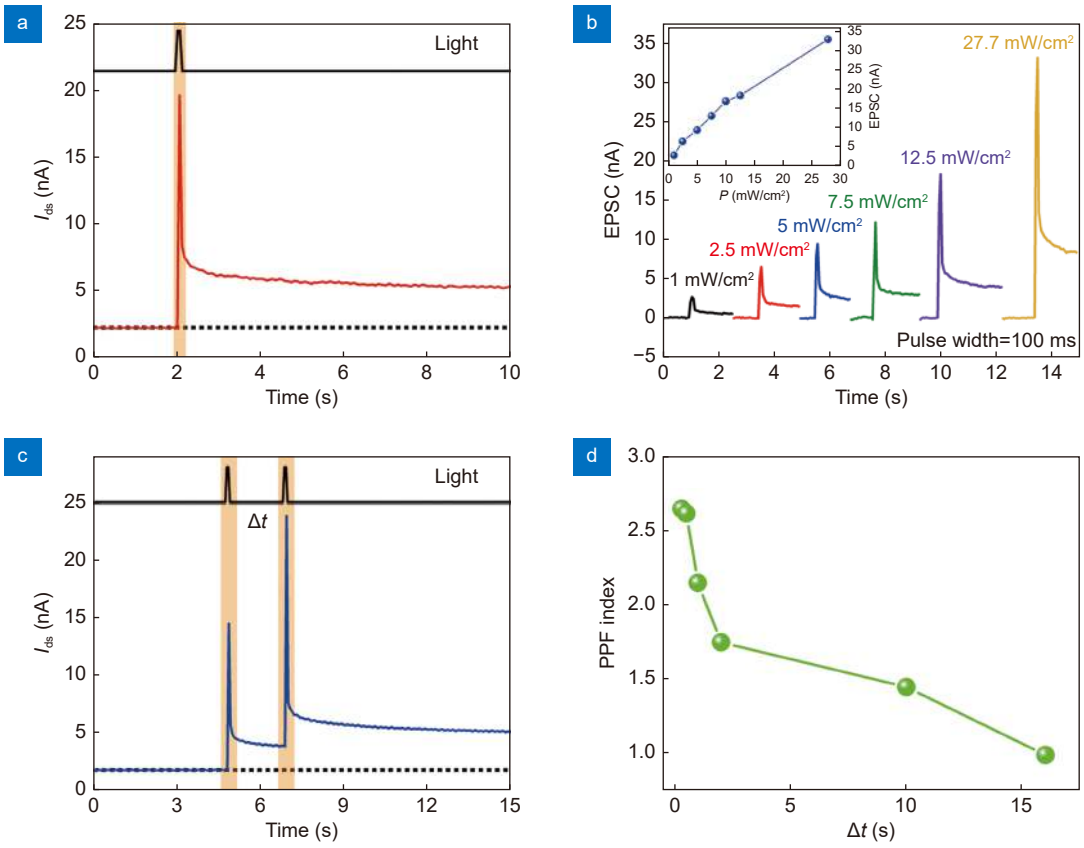

Fig. 3 | STP characteristics of the MoS_2 synaptic transistor. (**a**) The transient current response induced by an optical pulse of 50 ms. (**b**) The EPSC curves under different laser power densities (pulse width: 100 ms). Inset: The dependence of EPSC with differnent laser power densities (P). (**c**) The instantaneous current responses triggered by a pair of optical pulses (pulse width = 50 ms, pulse interval Δt = 2 s). The black dashed line represents the initial current in (a) and (c) without optical stimuli. (**d**) The PPF behaviors at different Δt.

rather than deep carrier traps at lower P[71]. Additionally, the sublinear relationship between EPSC and P in the inset of Fig.3(b) confirmed the presence of trap states further[72]. The sublinear relationship is attributed to the photogating effect[73] caused by long-lived charge trapping processes[71]. The PPF triggered by two consecutive presynaptic spikes at 2 s intervals is expressed in Fig. 3(c). A higher EPSC would be obtained after the second optical spike because of the effect of the first optical spike. The PPF index is defined as the ratio of A_2 to A_1 where A_2 and A_1 mean the EPSC triggered by the second or first light spike, respectively[18,74]. Figure 3(d) shows the PPF index increases as the pulse interval (Δt) decreases. This is in accordance with the behaviour of information processing in biological synapses[14]. Furthermore, the characteristic relaxation times of rapid and slow decay constants τ_1 and τ_2 can be estimated according to the double-exponential decay function given by Eq. (1)[18,75].

$$\text{PPF index} = C_1\exp(-\Delta t/\tau_1) + C_2\exp(-\Delta t/\tau_2) + C_0\ , \tag{1}$$

where C_0 equals to 1, which indicates the trend of PPF index is towards to 100% eventually[67]. In our case, the values of τ_1 and τ_2 are 0.8 s and 9.2 s fitted from Fig.3(d), respectively. Additionally, the age-related learning characteristics could be emulated by our synaptic transistors thanks to the PPF characteristics which are varied with human age[76].

Compared with STP, the LTP, i.e. long-term memory (LTM), usually takes longer time which means the lasting potentiation of the synaptic weight[12]. Figure 4(a–c) show the spike-number dependent LTP and forgetting behavior. The number of spikes could be regarded as the learning times[70]. There is a continuous upward trend of current as the number of spikes increases due to more and more photoinduced carriers. This is similar to biological synapses because successive stimuli could induce more neurotransmitters[6]. This phonomenon could explain more and more high-efficiency relearning behavior of a human's brain[39]. The forgetting behavior is liken by the EPSC after the optical spikes[14]. At first, the forgetting behavior would decrease rapidly and then decay slowly which is coincident with human brain[22,70]. As seen in Fig. 4(c), the delay of the transient current after photostimulation is fast at the beginning and then becomes slow. The delay speed is dependent on three continuous stages including recombination, shallow and deep trapping procedures[77]. The defect-induced recombination and traps make the corresponding fast and slow delay[78]. In addition, the spike-frequency dependent LTP and forgetting behavior are shown in Fig. 4(d–f). The higher frequency of repeated stimuli could enhance the synaptic weight and improve the memory function or learning efficiency obtained from Fig. 4(d)[17,76]. Moreover, the MoS_2 synaptic transistor shows the characteristic of the biological high-pass filters which could be applied for filtering unnecessary information in signal processing as

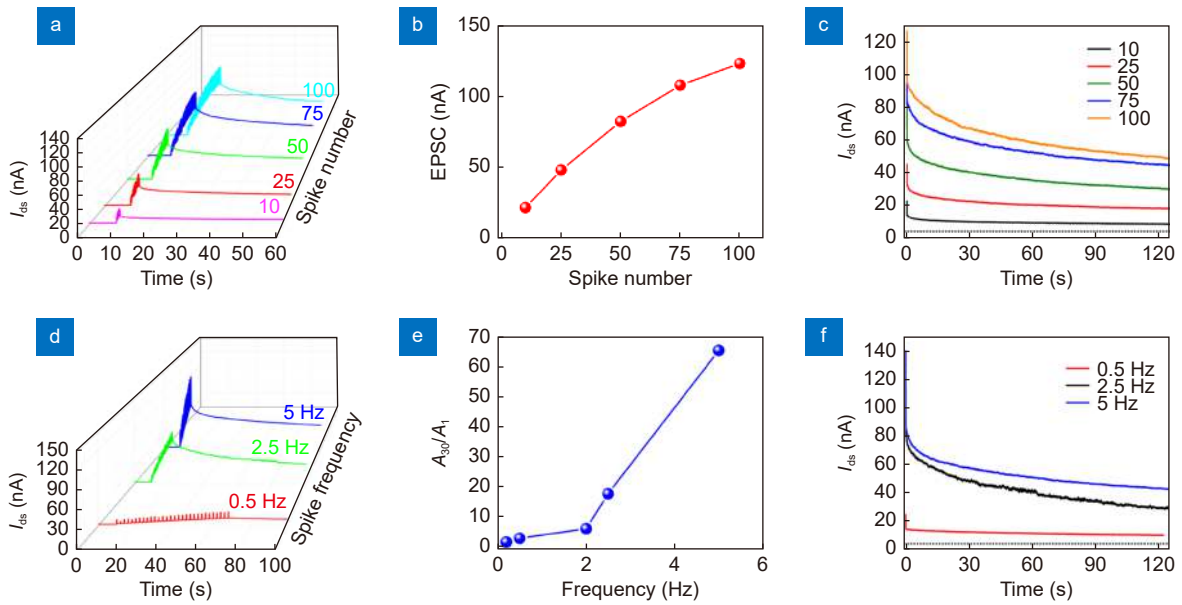

Fig. 4 | LTP characteristics of the MoS_2 synaptic transistor. The transient current (**a**), EPSC (**b**) and the extracted forgetting curve (**c**) from (a) after 10, 25, 50, 75 and 100 optical pulses. The transient current (**d**), A_{30}/A_1 (**e**) and the extracted forgetting curve (**f**) from (d) triggered by different spike frequency where A_{30} means the thirtieth EPSC. The black dashed line represents the initial current in (c) and (f) without optical stimuli.

shown in Fig. 4(e)[6,14,26,70]. The EPSC would become saturated eventually even though the number or frequency of optical pulses increases continuously. This means the synaptic device would not cause excessive neural activity[6]. From Fig. 4(c) and 4(f), the forgetting processes follow the classical Ebbinghaus forgetting curve which indicates the memory decays over time[79–81]. Furthermore, the higher-learning condition stimulated by more spike numbers or higher spike frequency leads to slower forgetting[82]. Note that the effect of single pulse duration time on synaptic plasticity is similar to spike number and the same is true for the Δt between two continuous stimuli and spike frequency[9].

The Pavlovian conditioning, as unconscious or procedural memory, could help creatures to be prepared for something expected or likely[13]. This process, a classical example of the associative learning, is consist of the acquisition, extinction and recovery[12]. The artificial synaptic devices could remember their past dynamic history, which is vital to mimic the Pavlovian conditioning[12,13]. Figure 5(a) shows the typical Pavlovian conditioning under one training. Here, the electrical spikes (E) of V_{ds} and light spikes (L) act as the bell and bones in the Pavlov's dog experiment. The bell ringing would make the dog salivate after the training of feeding and ringing bells together[13]. In Fig. 5(a) and 5(b), the black dashed line represents the threshold value of salivation. The EPSC under E would not reach the threshold value initially. However, the later E could induce salivation for the next five minutes after the stimuli of E and L together (E + L) shown in Fig. 5(a). In addition, 10 successive E + L spikes are applied as repeated trainings in Fig. 5(b). The EPSC maximum is far more than the threshold value after 10 spikes and the salivation state would last at least half an hour. This means the classical Pavlovian conditioning could be mimicked successfully based on our MoS_2 synaptic device and more trainings could make better associative learning.

The backgate (V_g) could regulate the memory function of our synaptic device as well except for repeated optical stimuli or electrical stimuli of V_{ds}[4,14,18,83]. Figure 5(c) and 5(d) depict the memory function of the synaptic transistor could be modulated by changing the V_g simply. It functions like the emotional effect on the memory function of human brain[84,85]. Figure 5(c) shows the small negative V_g of −0.1 V could significantly

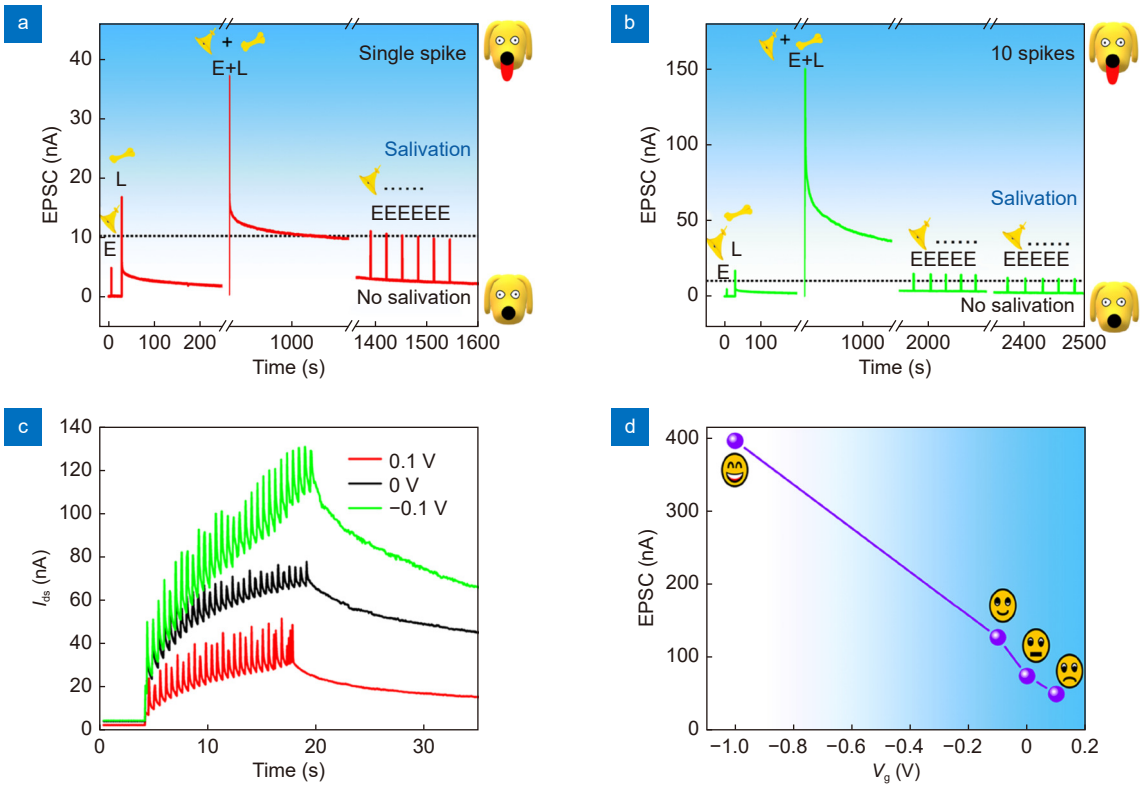

Fig. 5 | Schematic illustration of the Pavlovian conditioning and emotional effect on the MoS_2 synaptic transistor. The classical Pavlovian conditioning under one training (E+L) (**a**) and ten trainings (**b**). (**c**) The transient current triggered by 30 optical spikes at the backgate of 0.1 V, 0 V and –0.1 V. (**d**) The maximum EPSC at different V_g.

enhance the transient current under 30 optical spikes than that at zero gate voltage. On the contrary, the positive V_g could make the transient current decrease drastically. This phenomenon of increased EPSC may be attributed to negative gate voltage assisted detrapping of electrons. Cheng's group has reported that the free electron concentration or channel conductance increased due to released trapped electrons after negative gate voltage[86]. On the contrary, the positive gate voltage would make the free eletrons in the channel easier be trapped by trap centers resulting in the reduced channel conductance[86]. The inhibited current increment due to the applied positive gate voltage does not equate to the conventional inhibitory post-synaptic current[24,87]. The carrier trapping/detrapping under different positive/negative gate voltage is considered as the main operation mechanism of current switching behavior for the three-terminal artificial synapses[1,35,57]. The negative V_g could act like the positive emotions, and vice versa when positive V_g for our device. It is well-known that someone could have a better memory function in a good mood. A more obvious gate-tunable phenomenon is shown in Fig. 5(d). The EPSC would increase to about five times at the V_g of −1 V than that without V_g. Thus, our synaptic device could be applied for mimicking the visual learning and memory process at different emotions.

Inspired by human retina, our synaptic device would be further applied for neuromorphic imaging and preprocessing due to the excellent light-stimulated synaptic properties and easy large-area growth[41]. Figure 6(a) shows the schematic diagram of human's neuromorphic visual system. Given that, we stimulate the letter recognition of "I" under STP, LTP with or without -V_g shown in Fig. 6(b–d). The time needed for photocurrent decay to 1/e of its original state are 40 s and 2 min, respectively, for STP and LTP at zero V_g obtained from Fig. 6(b) and 6(c). The retention time of LTP is much longer than that of STP. The difference between LTP and STP is resulted from the different photo dosage which can make different effect on device conductance and decay dynamics[35].

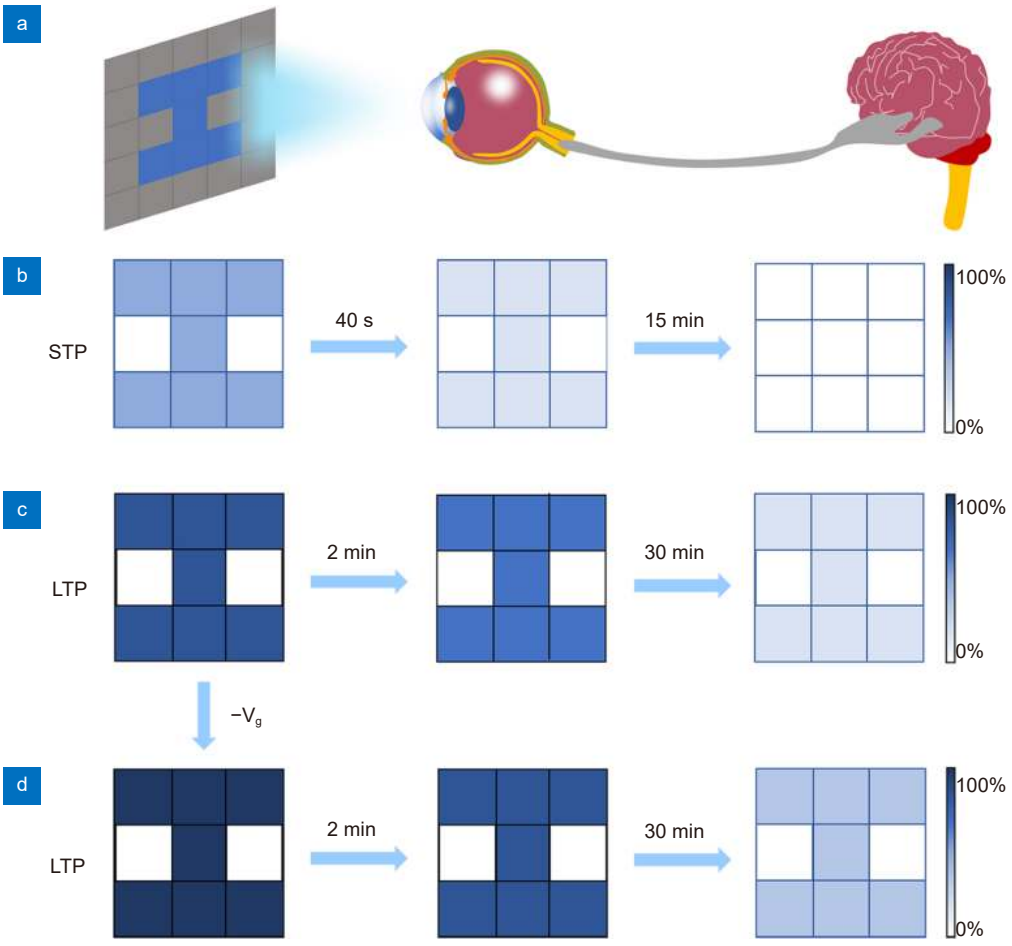

Fig. 6 | Neuromorphic imaging simulation. (**a**) Illustration of neuromorphic letter recognition. The stimulated letter recognition under STP (**b**), LTP with (**c**) or without (**d**) -V_g.

When the $-V_g$ was applied on the synaptic device, the photocurrent improved significantly in Fig. 6(d). Additionally, the big difference between STP and LTP makes the MoS_2 synaptic device show a better contrast in the pre-processing which is very important for efficient machine vision[15,41].

Conclusions

In summary, the uniform polycrystalline MoS_2 film could be a promising choice to mimic the visual perception and brain storage. The unique charge-trapping characteristics and facile synthesis of MoS_2 make it a favored candidate over other materials for bio-mimicking devices[1,17,18,37]. The photoreception capability of our device could expand the edge of vision from visible light to NIR light. Our photonic synapses could achieve information transfer and storage of the artificial brain with sensitive response to ultrashort optical pulses and the lowest power consumption under optical stimuli reported so far. The synaptic plasticity such as STP, PPF, LTP, forgetting behavior and associative learning are successful stimulated based on this proposed device. Moreover, the emotional effect on memory by regulating the backgate voltage is demonstrated. The channel conductance modulation is achieved by carrier trapping/detrapping in the channal and interfaces/surfaces[1]. Eventually, like the neuromorphic imaging and pre-processing device, the prospective imaging effect is shown. This work which integrates sensing-memory-preprocessing capabilities provides an insight into artificial retinal system and artificial brain.

Experimental section

CVD growth of MoS_2

The polycrystalline MoS_2 was grown in a 1 in. quartz tube with a one-zone furnace. Mixed MoO_3 powder (8.7 mg) and NaCl (1.4 mg) together placed in the center of the furnace and S powder (255 mg) were used as the precursor for the MoS_2 growth. A pair of Si/SiO_2 substrates are placed face to face with the vertical distance about 2 mm in the downstream after rinsing by acetone and isopropanol. The whole CVD process is controlled at a low pressure of 0.4 Torr (1 Torr=133.3223684 Pa) with the Ar/H_2 (8∶1) as the carrier gas after purging out the air in the tube about 10 min. The S powder is ramped up to 220 °C using a heating belt when the temperature of the furnace center reaching 670 °C. Then, the furnace was maintained for 30 min when it was heated up to 750 °C. Finally, the tube was cooled to room temperature naturally after removing the furnace.

Device fabrication

The Ti/Au (Ti: 10 nm, Au: 100 nm) metals were deposited by electron beam evaporation and then lifted off in acetone as the source and drain electrodes after the photolithography.

Material characterization

The optical images were captured by OLYMPUS microscope (LV100ND). The Raman and PL data were measured with a Raman-AFM confocal spectrometer (Witec, alpha300 RA) with a laser of 532 nm.

Device characterization

The optoelectronic properties of the photonic synapses were measured with the SemiProbe probe station and a semiconductor parameter analyzer (Keithley 4200) and Platform Design Automation (PDA, FS- Pro). Different duration of optical stimuli and different laser densities set by a Programmable DC Power Supply (Itech Electronic, IT6100B), a function generator and an irradiatometer were used to measure the photoresponse.

References

1. Pan X, Jin TY, Gao J, Han C, Shi YM et al. Stimuli-enabled artificial synapses for neuromorphic perception: progress and perspectives. *Small* **16**, 2001504 (2020).
2. Zhang QM, Yu HY, Barbiero M, Wang BK, Gu M. Artificial neural networks enabled by nanophotonics. *Light Sci Appl* **8**, 42 (2019).
3. Zhang K, Meng DL, Bai FM, Zhai JY, Wang ZL. Photon-memristive system for logic calculation and nonvolatile photonic storage. *Adv Funct Mater* **30**, 2002945 (2020).
4. Wu ZH, Lu JK, Shi T, Zhao XL, Zhang XM et al. A habituation sensory nervous system with memristors. *Adv Mater* **32**, 2004398 (2020).
5. Zhang JY, Dai SL, Zhao YW, Zhang JH, Huang J. Recent progress in photonic synapses for neuromorphic systems. *Adv Intell Syst* **2**, 1900136 (2020).
6. Zhang C, Wang SY, Zhao XL, Yang YH, Tong YH et al. Subfemtojoule-energy-consumption conformable synaptic transistors based on organic single-crystalline nanoribbons. *Adv Funct Mater* **31**, 2007894 (2021).
7. Kumarasinghe K, Kasabov N, Taylor D. Brain-inspired spiking neural networks for decoding and understanding muscle activity and kinematics from electroencephalography signals during hand movements. *Sci Rep* **11**, 2486 (2021).
8. Wang L, Liao WG, Wong SL, Yu ZG, Li SF et al. Artificial synapses based on multiterminal memtransistors for neuromorphic application. *Adv Funct Mater* **29**, 1901106 (2019).

9. Liu CS, Chen HW, Wang SY, Liu Q, Jiang YG et al. Two-dimensional materials for next-generation computing technologies. *Nat Nanotechnol* **15**, 545–557 (2020).
10. Zuo HR, Xu ZY, Zhang JL, Jia G. Visual tracking based on transfer learning of deep salience information. *Opto-Electron Adv* **3**, 190018 (2020).
11. Zhang L, Pan J, Zhang Z, Wu H, Yao N et al. Ultrasensitive skin-like wearable optical sensors based on glass micro/nanofibers. *Opto-Electron Adv* **3**, 190022 (2020).
12. Cheng YC, Li HJW, Liu B, Jiang LY, Liu M et al. Vertical 0D-perovskite/2D-MoS_2 van der Waals heterojunction phototransistor for emulating photoelectric-synergistically classical pavlovian conditioning and neural coding dynamics. *Small* **16**, 2005217 (2020).
13. Tan ZH, Yin XB, Yang R, Mi SB, Jia CL et al. Pavlovian conditioning demonstrated with neuromorphic memristive devices. *Sci Rep* **7**, 713 (2017).
14. Yin L, Huang W, Xiao RL, Peng WB, Zhu YY et al. Optically stimulated synaptic devices based on the hybrid structure of silicon nanomembrane and perovskite. *Nano Lett* **20**, 3378–3387 (2020).
15. Ahmed T, Tahir M, Low MX, Ren YY, Tawfik SA et al. Fully light-controlled memory and neuromorphic computation in layered black phosphorus. *Adv Mater* **33**, 2004207 (2021).
16. Gillick BT, Zirpel L. Neuroplasticity: an appreciation from synapse to system. *Arch Phys Med Rehabil* **93**, 1846–1855 (2012).
17. Wang TY, Meng JL, He ZY, Chen L, Zhu H et al. Ultralow power wearable heterosynapse with photoelectric synergistic modulation. *Adv Sci* **7**, 1903480 (2020).
18. Zhai YB, Zhou Y, Yang XQ, Wang F, Ye WB et al. Near infrared neuromorphic computing via upconversion-mediated optogenetics. *Nano Energy* **67**, 104262 (2020).
19. Majumdar S, Tan HW, Qin QH, van Dijken S. Energy-efficient organic ferroelectric tunnel junction memristors for neuromorphic computing. *Adv Electron Mater* **5**, 1800795 (2019).
20. Hebb DO. *The Organization of Behavior*: *A Neuropsychological Theory* (Psychology Press, London, 2005).
21. Bear MF, Connors BW, Paradiso MA. *Neuroscience Exploring the Brain* (Lippincott Williams & Wilkins, Philadelphia, 2007).
22. Xiao ZG, Huang JS. Energy-efficient hybrid perovskite memristors and synaptic devices. *Adv Electron Mater* **2**, 1600100 (2016).
23. Ma FM, Zhu YB, Xu ZW, Liu Y, Zheng XJ et al. Optoelectronic perovskite synapses for neuromorphic computing. *Adv Funct Mater* **30**, 1908901 (2020).
24. Han H, Yu HY, Wei HH, Gong JD, Xu WT. Recent progress in three-terminal artificial synapses: from device to system. *Small* **15**, 1900695 (2019).
25. Qian C, Oh S, Choi Y, Kim JH, Sun J et al. Solar-stimulated optoelectronic synapse based on organic heterojunction with linearly potentiated synaptic weight for neuromorphic computing. *Nano Energy* **66**, 104095 (2019).
26. Berco D, Ang DS, Zhang HZ. An optoneuronic device with realistic retinal expressions for bioinspired machine vision. *Adv Intell Syst* **2**, 1900115 (2020).
27. Park HL, Kim H, Lim D, Zhou HY, Kim YH et al. Retina-inspired carbon nitride-based photonic synapses for selective detection of UV light. *Adv Mater* **32**, 1906899 (2020).
28. Wei ZM, Li B, Xia CX, Cui Y, He J et al. Various structures of 2D transition-metal dichalcogenides and their applications. *Small Methods* **2**, 1800094 (2018).
29. Du W, Li CH, Sun JC, Xu H, Yu P et al. Nanolasers based on 2D materials. *Laser Photonics Rev* **14**, 2000271 (2020).
30. Zhao ZH, Wu D, Guo JW, Wu EP, Jia C et al. Synthesis of large-area 2D WS_2 films and fabrication of a heterostructure for self-powered ultraviolet photodetection and imaging applications. *J Mater Chem C* **7**, 12121–12126 (2019).
31. Zhang XM, Xiao SQ, Shi LH, Nan HY, Wan X et al. Large-size $Mo_{1-x}W_xS_2$ and $W_{1-x}Mo_xS_2$ (x = 0–0.5) monolayers by confined-space chemical vapor deposition. *Appl Surf Sci* **457**, 591–597 (2018).
32. Akinwande D, Huyghebaert C, Wang CH, Serna MI, Goossens S et al. Graphene and two-dimensional materials for silicon technology. *Nature* **573**, 507–518 (2019).
33. Fang MX, Wang F, Han YM, Feng YL, Ren TL et al. Controlled growth of bilayer-MoS_2 films and MoS_2-based field-effect transistor (FET) performance optimization. *Adv Electron Mater* **4**, 1700524 (2018).
34. Wu M, Xiao YH, Zeng Y, Zhou YL, Zeng XB et al. Synthesis of two-dimensional transition metal dichalcogenides for electronics and optoelectronics. *InfoMat* **3**, 362–396 (2021).
35. Feng XW, Liu XK, Ang KW. 2D photonic memristor beyond graphene: progress and prospects. *Nanophotonics* **9**, 1579–1599 (2020).
36. Li ZW, Yang W, Huang M, Yang X, Zhu CG et al. Light-triggered interfacial charge transfer and enhanced photodetection in CdSe/ZnS quantum dots/MoS_2 mixed-dimensional phototransistors. *Opto-Electron Adv* **4**, 210017 (2021).
37. Sup Choi M, Lee GH, Yu YJ, Lee DY, Hwan Lee S et al. Controlled charge trapping by molybdenum disulphide and graphene in ultrathin heterostructured memory devices. *Nat Commun* **4**, 1624 (2013).
38. Hu YX, Dai MJ, Feng W, Zhang X, Zhang SC et al. Monolayer hydrophilic MoS_2 with strong charge trapping for atomically thin neuromorphic vision systems. *Mater Horiz* **7**, 3316–3324 (2020).
39. Huang W, Xia XW, Zhu C, Steichen P, Quan WD et al. Memristive artificial synapses for neuromorphic computing. *Nano-Micro Lett* **13**, 85 (2021).
40. Gao CF, Lee MP, Li MJ, Lee KC, Yang FS et al. Mimic drug dosage modulation for neuroplasticity based on charge-trap layered electronics. *Adv Funct Mater* **31**, 2005182 (2021).
41. Choi C, Leem J, Kim MS, Taqieddin A, Cho C et al. Curved neuromorphic image sensor array using a MoS_2-organic heterostructure inspired by the human visual recognition system. *Nat Commun* **11**, 5934 (2020).
42. Qin SC, Wang FQ, Liu YJ, Wan Q, Wang XR et al. A light-stimulated synaptic device based on graphene hybrid phototransistor. *2D Mater* **4**, 035022 (2017).
43. Kumar M, Abbas S, Kim J. All-oxide-based highly transparent photonic synapse for neuromorphic computing. *ACS Appl Mater Interfaces* **10**, 34370–34376 (2018).
44. Chen TQ, Wang X, Hao DD, Dai SL, Ou QQ et al. Photonic synapses with ultra-low energy consumption based on vertical organic field-effect transistors. *Adv Opt Mater* **9**, 2002030

(2021).

45. Xiao M, Wang HD, Liu JF, Yang H, Zhang H. Artificial visual memory device based on a photo-memorizing composite and one-step manufacturing. *Mater Horiz* **7**, 1597–1604 (2020).
46. Zhu JT, Li W, Huang R, Ma L, Sun HM et al. One-pot selective epitaxial growth of large WS_2/MoS_2 lateral and vertical heterostructures. *J Am Chem Soc* **142**, 16276–16284 (2020).
47. Ganger ZD. Growth of two-dimensional molybdenum disulfide via chemical vapor deposition (Wright State University, Dayton, 2019).
48. Hong S, Zagni N, Choo S, Liu N, Baek S et al. Highly sensitive active pixel image sensor array driven by large-area bilayer MoS_2 transistor circuitry. *Nat Commun* **12**, 3559 (2021).
49. Lee HS, Min SW, Chang YG, Park MK, Nam T et al. MoS_2 nanosheet phototransistors with thickness-modulated optical energy gap. *Nano Lett* **12**, 3695–3700 (2012).
50. Choi W, Cho MY, Konar A, Lee JH, Cha GB et al. High-detectivity multilayer MoS_2 phototransistors with spectral response from ultraviolet to infrared. *Adv Mater* **24**, 5832–5836 (2012).
51. Ren AB, Zou JH, Lai HG, Huang YX, Yuan LM et al. Direct laser-patterned MXene–perovskite image sensor arrays for visible-near infrared photodetection. *Mater Horiz* **7**, 1901–1911 (2020).
52. Yang ZB, Hao JH, Lau SP. Synthesis, properties, and applications of 2D amorphous inorganic materials. *J Appl Phys* **127**, 220901 (2020).
53. Bittle EG, Basham JI, Jackson TN, Jurchescu OD, Gundlach DJ. Mobility overestimation due to gated contacts in organic field-effect transistors. *Nat Commun* **7**, 10908 (2016).
54. Fashandi H, Dahlqvist M, Lu J, Palisaitis J, Simak SI et al. Synthesis of Ti_3AuC_2, $Ti_3Au_2C_2$ and Ti_3IrC_2 by noble metal substitution reaction in Ti_3SiC_2 for high-temperature-stable Ohmic contacts to SiC. *Nat Mater* **16**, 814–818 (2017).
55. Wang Y, Kim JC, Wu RJ, Martinez J, Song XJ et al. Van der Waals contacts between three-dimensional metals and two-dimensional semiconductors. *Nature* **568**, 70–74 (2019).
56. Shen PC, Su C, Lin YX, Chou AS, Cheng CC et al. Ultralow contact resistance between semimetal and monolayer semiconductors. *Nature* **593**, 211–217 (2021).
57. Zhou FC, Chen JW, Tao XM, Wang XR, Chai Y. 2D materials based optoelectronic memory: convergence of electronic memory and optical sensor. *Research* **2019**, 9490413 (2019).
58. Jonsson A, Sjöström TA, Tybrandt K, Berggren M, Simon DT. Chemical delivery array with millisecond neurotransmitter release. *Sci Adv* **2**, e1601340 (2016).
59. Hao DD, Zhang JY, Dai SL, Zhang JH, Huang J. Perovskite/organic semiconductor-based photonic synaptic transistor for artificial visual system. *ACS Appl Mater Interfaces* **12**, 39487–39495 (2020).
60. Tu LQ, Cao RR, Wang XD, Chen Y, Wu SQ et al. Ultrasensitive negative capacitance phototransistors. *Nat Commun* **11**, 101 (2020).
61. Wang X, Lu Y, Zhang JY, Zhang SQ, Chen TQ et al. Highly sensitive artificial visual array using transistors based on porphyrins and semiconductors. *Small* **17**, 2005491 (2021).
62. Meng Y, Li FZ, Lan CY, Bu XM, Kang XL et al. Artificial visual systems enabled by quasi–two-dimensional electron gases in oxide superlattice nanowires. *Sci Adv* **6**, eabc6389 (2020).
63. Wang Y, Lv ZY, Chen JR, Wang ZP, Zhou Y et al. Photonic synapses based on inorganic perovskite quantum dots for neuromorphic computing. *Adv Mater* **30**, 1802883 (2018).
64. Ahmed T, Kuriakose S, Mayes ELH, Ramanathan R, Bansal V et al. Optically stimulated artificial synapse based on layered black phosphorus. *Small* **15**, 1900966 (2019).
65. Pradhan B, Das S, Li JX, Chowdhury F, Cherusseri J et al. Ultrasensitive and ultrathin phototransistors and photonic synapses using perovskite quantum dots grown from graphene lattice. *Sci Adv* **6**, eaay5225 (2020).
66. Jiang J, Hu WN, Xie DD, Yang JL, He J et al. 2D electric-double-layer phototransistor for photoelectronic and spatiotemporal hybrid neuromorphic integration. *Nanoscale* **11**, 1360–1369 (2019).
67. Wang SY, Chen CS, Yu ZH, He YL, Chen XY et al. A MoS_2/PTCDA hybrid heterojunction synapse with efficient photoelectric dual modulation and versatility. *Adv Mater* **31**, 1806227 (2019).
68. Cheng ZG, Ríos C, Pernice WHP, Wright CD, Bhaskaran H. On-chip photonic synapse. *Sci Adv* **3**, e1700160 (2017).
69. Zhao YY, Sun WJ, Wang J, He JH, Li H et al. All-inorganic ionic polymer-based memristor for high-performance and flexible artificial synapse. *Adv Funct Mater* **30**, 2004245 (2020).
70. Wang K, Dai SL, Zhao YW, Wang Y, Liu C et al. Light-stimulated synaptic transistors fabricated by a facile solution process based on inorganic perovskite quantum dots and organic semiconductors. *Small* **15**, 1900010 (2019).
71. Kufer D, Konstantatos G. Highly sensitive, encapsulated MoS_2 photodetector with gate controllable gain and speed. *Nano Lett* **15**, 7307–7313 (2015).
72. Zhao QH, Wang W, Carrascoso-Plana F, Jie WQ, Wang T et al. The role of traps in the photocurrent generation mechanism in thin InSe photodetectors. *Mater Horiz* **7**, 252–262 (2020).
73. Guo JM, Wen RM, Zhai JY, Wang ZL. Enhanced NO_2 gas sensing of a single-layer MoS_2 by photogating and piezo-phototronic effects. *Sci Bull* **64**, 128–135 (2019).
74. Zhao XN, Xu HY, Wang ZQ, Lin Y, Liu YC. Memristors with organic-inorganic halide perovskites. *InfoMat* **1**, 183–210 (2019).
75. Zucker RS, Regehr WG. Short-term synaptic plasticity. *Annu Rev Physiol* **64**, 355–405 (2002).
76. Lee KC, Li MJ, Chang YH, Yang SH, Lin CY et al. Inverse paired-pulse facilitation in neuroplasticity based on interface-boosted charge trapping layered electronics. *Nano Energy* **77**, 105258 (2020).
77. Simmons JG, Taylor GW. Nonequilibrium steady-state statistics and associated effects for insulators and semiconductors containing an arbitrary distribution of traps. *Phys Rev B* **4**, 502–511 (1971).
78. Jiang J, Ling CY, Xu T, Wang WH, Niu XH et al. Defect engineering for modulating the trap states in 2D photoconductors. *Adv Mater* **30**, 1804332 (2018).
79. Ebbinghaus H. *Uber das Gedächtnis*: *Untersuchungen zur Experimentellen Psychologie* (Duncker & Humber, Leipzig, 1885).
80. Laborieux A, Ernoult M, Hirtzlin T, Querlioz D. Synaptic metaplasticity in binarized neural networks. *Nat Commun* **12**, 2549 (2021).

81. Wang Y, Yin L, Huang W, Li YY, Huang SJ et al. Optoelectronic synaptic devices for neuromorphic computing. *Adv Intell Syst* **3**, 2000099 (2021).
82. Loftus GR. Evaluating forgetting curves. *J Exp Psychol Learn Mem Cogn* **11**, 397–406 (1985).
83. Zhang ZZ, Wang ZW, Shi T, Bi C, Rao F et al. Memory materials and devices: from concept to application. *InfoMat* **2**, 261–290 (2020).
84. Rolls ET, Stringer SM. A model of the interaction between mood and memory. *Netw Comput Neural Syst* **12**, 89–109 (2001).
85. Bryan T, Mathur S, Sullivan K. The impact of positive mood on learning. *Learn Disabil Quart* **19**, 153–162 (1996).
86. Zou JY, Cai ZY, Lai YJ, Tan JY, Zhang RJ et al. Doping concentration modulation in vanadium-doped monolayer molybdenum disulfide for synaptic transistors. *ACS Nano* **15**, 7340–7347 (2021).
87. Wang SY, Liu L, Gan LR, Chen HW, Hou X et al. Two-dimensional ferroelectric channel transistors integrating ultra-fast memory and neural computing. *Nat Commun* **12**, 53 (2021).

Acknowledgements

This work was financially supported by the National Key Research and Development Program of China (2019YFB2203400), the "111 Project" (B20030), the UESTC Shared Research Facilities of Electromagnetic Wave and Matter Interaction (Y0301901290100201), the Fundamental Research Funds for the Central Universities (ZYGX2019Z018), the National Natural Science Foundation of China (61974014), and the Innovation Group Project of Sichuan Province (20CXTD0090).

Author contributions

C. H. Li, W. Du and J. Wu conceived and designed the research project. C. H. Li synthesized the samples and performed the optical spectroscopy. J. H. Zou and S. Sun helped the photolithography process. C. H. Li fabricated the device and carried out the optoelectronic measurements with the help of W. Du. L. Z. Luo participated in setting up the measurements. C. H. Li analyzed the data and wrote the manuscript with the contribution from Y. X. Huang and J. Wu. A. O. Govorov revised the manuscript. J. Wu, H. X. Xu and Z. M. Wang supervised the project and revised the manuscript.

Competing interests

The authors declare no competing financial interests.